

1       **Explainable artificial intelligence in geoscience: a**  
2       **glimpse into the future of landslide susceptibility**  
3       **modeling**

4                               **Ashok Dahal<sup>1</sup>, Luigi Lombardo<sup>1</sup>**

5       <sup>1</sup>University of Twente, Faculty of Geo-Information Science and Earth Observation (ITC), PO Box 217,  
6                               Enschede, AE 7500, Netherlands

7       **Key Points:**

- 8       • A new generation of interpretable machine learning models is tested and presented  
9       to predict landslide occurrences.
- 10      • The traditional definition of black box is left in favor of tools that can be queried  
11      to understand the artificially intelligent decision.
- 12      • A web-GIS platform has also been developed to showcase the potential of explain-  
13      able artificial intelligence for geoscientific applications.

---

Corresponding author: Ashok Dahal, [a.dahal@utwente.nl](mailto:a.dahal@utwente.nl)

## Abstract

For decades, the distinction between statistical models and machine learning ones has been clear. The former are optimized to produce interpretable results, whereas the latter seeks to maximize the predictive performance of the task at hand. This is valid for any scientific field and for any method belonging to the two categories mentioned above. When attempting to predict natural hazards, this difference has lead researchers to make drastic decisions on which aspect to prioritize, a difficult choice to make. In fact, one would always seek the highest performance because at higher performances correspond better decisions for disaster risk reduction. However, scientists also wish to understand the results, as a way to rely on the tool they developed. Today, very recent development in deep learning have brought forward a new generation of interpretable artificial intelligence, where the prediction power typical of machine learning tools is equipped with a level of explanatory power typical of statistical approaches. In this work, we attempt to demonstrate the capabilities of this new generation of explainable artificial intelligence (ExAI). To do so, we take the landslide susceptibility context as reference. Specifically, we build an ExAI trained to model landslides occurred in response to the Gorkha earthquake (25 April 2015), providing an educational overview of the model design and its querying opportunities. The results are surprising, the performance are extremely high, while the interpretability can be extended to the probabilistic result assigned to single mapping units. This is also showcased in a web-GIS (<https://arcg.is/0unziD>) platform we built.

## 1 Introduction

The evolution of science is marked by historical moments where discoveries or technological advancements opened up opportunities that were not there before. The history of geoscience and specifically the part of it linked to natural hazards is no different. Specifically, if we take the landslide example, before 1970's no available study attempted to estimate locations where landslides were likely to occur over a large landscape. This notion was later defined as landslide susceptibility (Reichenbach et al., 2018) and its first example dates back to Brabb et al. (1972), with a digital scan of his susceptibility map still being accessible at this link (<https://pubs.usgs.gov/mf/0360/plate-1.pdf>). The introduction of that document had effect that rippled even to present days. Specifically, it set the stage for a successful branch of geomorphology that has received wide attention and efforts since then. One of the main issues that document had was the fact that it relied on expert-based opinions. In other words, the definition of susceptibility classes was the result of a subjective decision. Few years later though, the introduction of Geographic Information Systems (GIS; Gates & Heil, 1980) laid the foundations to collect digital cartographic data and implement numerical operations. As a result, the geomorphological community was able to test data-driven approaches suitable to move past the subjectivity issue. This later led to the first introduction of bivariate statistical models (Naranjo et al., 1994; Soeters & Van Westen, 1994) and their multivariate extension (P. Atkinson et al., 1998; P. M. Atkinson & Massari, 1998). The latter still constitute the most common method to estimate landslide susceptibility (Reichenbach et al., 2018). Their success is due to the satisfying performance they demonstrated through the years and their high level of interpretability. The way they work is to assume a vector of landslide presence/absence data to behave across the geographic space according to a Bernoulli probability distribution, whose relation to the landslide is linearly related to a set of covariates. The latter are usually referred to as predisposing or triggering factors (Das et al., 2012; Tanyaş et al., 2022). However, the linearity assumption these models are based on, limited the performance one could obtain. Therefore, another moment of particular importance was the introduction of machine learning tools (e.g., Yesilnacar & Topal, 2005). Even the simplest of them allowed for linear combinations of nonlinear relations, providing good flexibility and performance. This is the main reason why a multitude of scientific contributions got published since then, testing each one of these new

67 approaches, from neural network (Melchiorre et al., 2008), to decision trees (Li & Clara-  
68 munt, 2006) and their subsequent stochastic versions (Vorpahl et al., 2012; Catani et al.,  
69 2013), and from support vector machines (Ballabio & Sterlacchini, 2012) to multivari-  
70 ate adaptive regression splines (Marmion et al., 2009). All these newly introduced meth-  
71 ods though, lacked in interpretability, which is why conventional statistical models still  
72 kept on being the most common modeling choice. Moreover, even statistical models re-  
73 ceived a boost in their allowed complexity, as contributions based on generalized addi-  
74 tive models began to flourish (Brenning, 2008; J. N. Goetz et al., 2011). Since, then the  
75 two applications reached a sort of stalemate, where machine learning tool were sought  
76 for performance and statistical ones for interpretation. This is reflected even nowadays,  
77 after a decade, through the number of comparative studies, where the results of one or  
78 the other option are constantly tested to discern advantages and disadvantages (Pourghasemi  
79 & Rossi, 2017; J. Goetz et al., 2015).

80 The very same period has also witnessed improvements in the choice of the geo-  
81 graphic object to partition an area under study, with unique condition units (Bednarik  
82 & Pauditiš, 2010; Titti et al., 2021), slope units (Carrara, 1983; Alvioli et al., 2016) and  
83 grid cells (Dhakal et al., 2000; P. M. Atkinson & Massari, 1998) becoming the most com-  
84 mon choices, in ascending order (Reichenbach et al., 2018).

85 Notably, the recent introduction of deep learning architectures has further set apart  
86 the statistical and data mining applications for landslide prediction. The classification  
87 performance of tools such as Convolutional Neural Network (Yi et al., 2020) have been  
88 shown to be even higher than their traditional machine learning counterparts (Bui et al.,  
89 2020; Fang et al., 2020) attracting the attention of a large part of the community although  
90 this is still achieved at the expense of interpretation capacity. And, their use further sup-  
91 ported the grid cell partition because convolutional operations are commonly based on  
92 a lattice structure (Van Dao et al., 2020), with the exception of few deep learning stud-  
93 ies adopting slope units (Hua et al., 2021).

94 In this complex system though, a new moment will soon mark the evolution that  
95 landslide susceptibility models have undergone since Brabb et al. (1972). Information  
96 science has put forward a huge effort to give machine learning tools the same interpre-  
97 tation capacity of statistically based models (Štrumbelj & Kononenko, 2014; Ribeiro et  
98 al., 2016). This has recently resulted in the seminal work of Lundberg and Lee (2017).  
99 Specifically, the authors have built the first artificial intelligence that can be queried on  
100 an element by element basis as well as a predictor by predictor basis. In other words,  
101 their model can be dissected to the level of each components it has been built upon and  
102 the results can be examined to the point of understanding why the algorithm converged  
103 to assign a specific label to a specific unit. This in an unprecedented achievement, for  
104 it opens up an entirely new field of applications in any other scientific field. In the con-  
105 text of landslide prediction, this can finally unify a modeling framework from which de-  
106 rive standard practices for susceptibility modeling. Being a complete new breakthrough,  
107 the present manuscript attempts to showcase the potential of Explainable Artificial In-  
108 telligence (ExAI, hereafter) for landslide susceptibility modeling. The remainder of the  
109 manuscript does so by providing context on the basis of the landslides triggered by the  
110 Gorkha earthquake. Moreover, a web application is also shared with the readers allow-  
111 ing them to explore and get accustomed to the potential of this new generation mod-  
112 els.

## 113 2 Materials and Methods

114 Below, Section 2.1 will provide an overview of the data used in this work to demon-  
115 strate the potential of ExAI, whose design and web app graphical interface are presented  
116 in Section 2.2 and 2.4, respectively.

117

## 2.1 Data

118

### 2.1.1 Landslide inventory

119

120

121

122

123

124

We tested our ExAI in the area struck by the Gorkha earthquake ( $7.8 M_w$ ) on the 25<sup>th</sup> of April 2015. Roback et al. (2017) mapped 24,903 coseismic landslides for this event, and presented their characteristics in Roback et al. (2018), with a total landslide area of 86.5 km<sup>2</sup> (Nowicki Jessee et al., 2018). Figure 1 The polygonal inventory is freely accessible at the global database of earthquake-induced landslide inventories (Tanyaş et al., 2017).

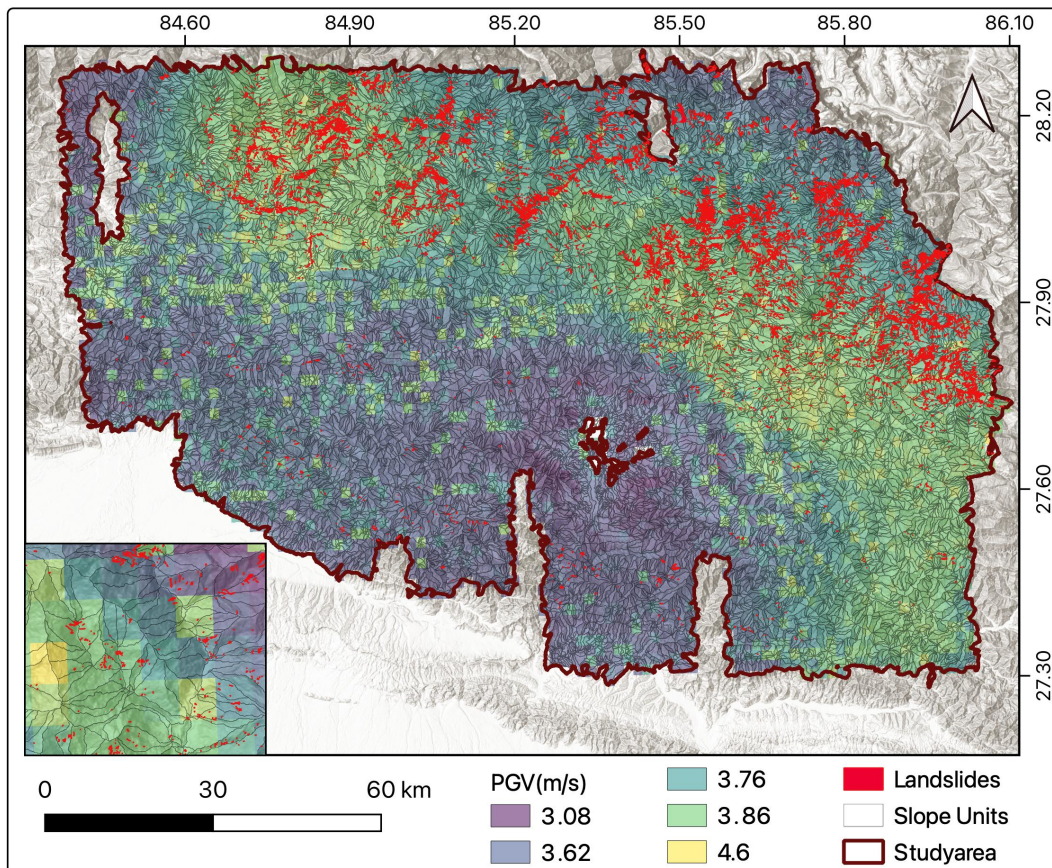


**Figure 1.** Overview of the study area, coseismic ground motion and associated landslides. The small panel to the bottom left shows a detail of the spatial partition we used, later explained in Section 2.1.2

125

126

127

Notably, this inventory is among the best coseismic ones for its quality and completeness (Tanyaş & Lombardo, 2020) for the authors characterize the polygon into source and deposition areas.

128

129

130

In this work, we use the spatial signal carried by this inventory as the target variable of our susceptibility model, aggregated at the level of slope units (more details below).

### 131 **2.1.2 Slope unit partition**

132 Slope units (SU) are irregular polygonal objects bound between ridges and stream-  
 133 lines (Carrara et al., 1995). Their use is an alternative to grid cells, which is particularly  
 134 suited for regional scale susceptibility models. The recent introduction of the *r.slopeunits*  
 135 software by Alvioli et al. (2016) is able to quickly generate SU under the constraint of  
 136 slope exposition homogeneity, thus requiring only a digital elevation model as input data,  
 137 and a few parameters to control the subdivision process. In our case, we opted for the  
 138 latest version of *r.slopeunits*, capable of returning a reliable partition removing flat or  
 139 near-flat areas (e.g., Alvioli et al., 2020; Lombardo & Tanyas, 2021).

140 Here we opted to run *r.slopeunits* with the following parameterization (after run-  
 141 ning a number of unreported tests): `area_min=40000`, `circular_variance=0.4`, `cleansize=20000`,  
 142 `thresh=800000`. These parameters control certain aspects of the calculations at the core  
 143 of *r.slopeunits*. Specifically: *a*) `area_min` indicates the minimum SU area to coverge to;  
 144 *b*) the circular variance controls how flexible or rigid the aspect criterion should be, with  
 145 0 being extremely rigid and 1 allowing for a large within-SU variability; *c*) `cleansize` refers  
 146 to the dimension of spurious SU to be merged to the neighboring polygons; *d*) `thresh`  
 147 is the SU extent *r.slopeunits* should start from.

148 This routine returned 16533 SU, with a mean planimetric area of  $8.6 \times 10^5$  km<sup>2</sup> and  
 149 a standard deviation of  $7.8 \times 10^5$  km<sup>2</sup>. These summary statistics attest for a slightly coarse  
 150 resolution of the SU, which we opted for simply for computational reasons. In fact, as  
 151 we planned to share a web-GIS platform where our model can be interactively queried,  
 152 a finer SU partition would have implied a much slower interface.

### 153 **2.1.3 Predictors**

154 Our model relies on a set of predictors we chose to explain the predisposing and  
 155 triggering factors that have led to the coseismic inventory mapped by Roback et al. (2017).  
 156 Specifically, we opted for eight predictors, the morphometric ones originating from the  
 157 30 m SRTM digital elevation model (Van Zyl, 2001). These encompass: *i*) Slope steep-  
 158 ness (*Slp*; Zevenbergen & Thorne, 1987); *ii*) horizontal (*Hc* Heerdegen & Beran, 1982)  
 159 and *iii*) vertical (*Vc* Heerdegen & Beran, 1982) curvatures; *iv*) Eastness (*Est*) and *Nrt*)  
 160 Northness (Lombardo et al., 2018). As for the expression of the *vi*) ground motion in  
 161 terms of Peak Ground Velocity (*PGV\_Usgs*), this came from the ShakeMap system of  
 162 the United States Geological Survey (Worden & Wald, 2016). Vegetation density was  
 163 brought in via Normalized Difference Vegetation Index (NDVI) (Pettorelli et al., 2005),  
 164 computed from Landsat Imagery (Survey, 2015), whereas the antecedent precipitation  
 165 (*Prc*) was calculated as accumulated rain over a three months period prior to the earth-  
 166 quake occurrence, from CHIRPS data (Funk et al., 2015).

167 The spatial pattern of these covariates was aggregated at the SU level by taking  
 168 the mean value within the given SU, something highlighted in the remainder of the text  
 169 with the suffix “\_m”. Notably, it is customary to express the variability of a given pre-  
 170 dictor within a SU by taking its mean behaviour as well as its variance for near Gaus-  
 171 sian distributions (Guzzetti et al., 2006; Lombardo & Tanyas, 2020), or to use a quan-  
 172 tile representation in situation far from the normality assumption (Castro Camilo et al.,  
 173 2017; Amato et al., 2019). However, here to keep the model simple and easy to be ex-  
 174 plained, we opted to avoid adding the variability of each predictor per SU. Our expla-  
 175 nation is that we are not trying to reach high performance through deep learning, this  
 176 is something already shown in a number of contributions (e.g., Meena et al., 2022). Con-  
 177 versely, we seek to demonstrate the power of ExAI in susceptibility modeling.

178 As the last preprocessing step, we normalized all predictors between zero and one  
 179 using the following transformation for each predictor:

$$X_{norm} = (X_{original} - \min(X_{original})) / (\max(X_{original}) - \min(X_{original})) \quad (1)$$

## 2.2 Explainable AI design

The deep learning model we used to test our Explainable AI was kept simple to easily diagnose the model output and to prevent it from overfitting. Its basic structure is shown in Figure 2, where the model relies on 8 input features in the input layer, followed by 12 hidden layers made out of fully connected layers of size 64 and a output layer with a sigmoid activation function. Each hidden layer is accompanied by a Rectified Linear Unit (ReLU) non linear activation (Yarotsky, 2017), followed by batch normalization (Ioffe & Szegedy, 2015) and a dropout layer (Baldi & Sadowski, 2013) with 0.3% dropout. These three elements have nowadays become standard in most deep learning architectures and we refer to the work of Schmidhuber (2015) for further details. For conciseness, here we will briefly mention that the ReLU activation allows for the model to be flexible and incorporate non-linear behaviors. Moreover, the dropout layer is used to prevent overfitting, whereas the batch normalization layer prevents weights and biases to grow unrealistically.

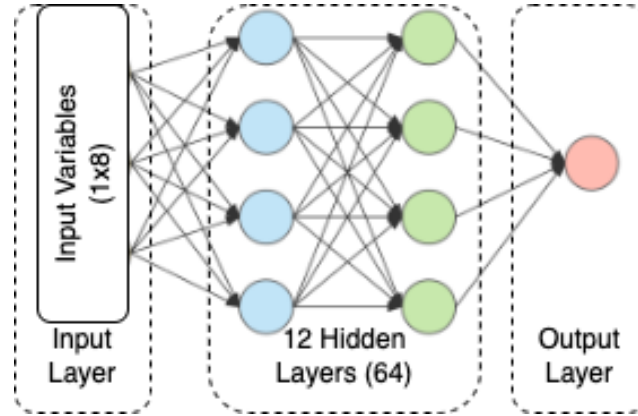


**Figure 2.** Simple architecture of the landslide susceptibility model which is used in our ExAI.

To train our model, we used the dataset as described in the section 2.1. The dataset was randomly divided into two disjoint training (70%) and test (30%) set. The training set was further randomly divided into 20% validation set which was randomly selected with replacement in each training epoch. All of the training performance were evaluated in the validation set (for e.g. training performance) and the model's performance itself was evaluated with the test set.

The developed model is trained using weighted binary crossentropy loss function, due to imbalance in the landslide data we provided  $4\times$  higher weights to the positive outcomes (landslides). The weight set to 4 because amount of slope-units with landslide was around 20% and without landslide was around 80%. To train the model we used Adam optimizer (Kingma & Ba, 2014) with initial learning rate of  $1\times 10^{-3}$  and decayed exponentially at 10000 training steps with decay rate of 0.9. The training was done with the batch size of 32 for 500 epochs with an early stopping option. This implies that the training process automatically stops once the model tends to overfit.

Once the model was fully trained and shown good performance, we calculated SHapley Additive exPlanations (SHAP) values to diagnose the model and its decisions (Lundberg & Lee, 2017). The SHAP values are calculated using the DeepSHAP method developed

211 by Lundberg and Lee (2017). To provide a explanation about SHAP values below we  
 212 present a simple practical example. Let us assume we are in the context of a simple lin-  
 213 ear regression where the target variable is regressed against only three covariates. The  
 214 relative equation could be denoted as:

$$Y = \sum \beta_0 + \beta_1 X_1 + \beta_2 X_2 + \beta_3 X_3 \quad (2)$$

215 Interpreting such simple model would be an easy task as it boils down to a linear  
 216 combination of linear relations. However, machine/deep learning architectures offer the  
 217 ability to extent the modeling framework even towards nonlinear combination of non-  
 218 linear relations, which is something that makes the interpretation a very difficult task.  
 219 For this reason, what SHAP does is to solve the predictive equation for each mapping  
 220 unit of interest and storing the relative results. This provides a unique perspective on  
 221 each predictor's role with respect to the others, for each slope unit in our case. In other  
 222 words, to compute SHAP, one has to take the weights estimated for each predictors, mul-  
 223 tiple them for the actual predictors value and then combine them for each element in  
 224 the matrix. These can then be stored and queried later on to understand how a specific  
 225 probability value has been assigned to a slope unit. In the linear example mentioned above  
 226 and for a single mapping unit, this would allow starting from the initial intercept value  
 227  $\beta_0$  then adding the term that contributes the least to the final estimate (say  $\beta_2 X_2$ ), then  
 228 adding the second (say  $\beta_3 X_3$ ) and the third (say  $\beta_1 X_1$ ). As a result, SHAP allows to  
 229 see changes in probability estimates as a function of each predictor offering a unique as-  
 230 sessment tool on the final estimates and how the model has reached them.

### 231 **2.3 Performance assessment**

232 Aside from the added interpretability value of our ExAI, understanding how well  
 233 it labels slope units into stable or unstable is a fundamental requirement of any binary  
 234 classifier. Here, we monitored the ExAI performance via Receiver Operating Character-  
 235 istic (ROC) curves and their Area Under the CURve (AUC) as per standard (Hosmer &  
 236 Lemeshow, 2000; Rahmati et al., 2019). We used this cutoff-independent metric while  
 237 testing our model over different data realizations. In addition, we also produced cutoff-  
 238 dependent metrics by taking the median of the probability distribution. This operation  
 239 ensures the conversion of the continuous probability spectrum into two classes (stable/unstable  
 240 slopes) which can be further matched to the original data to estimate True Positives (TP),  
 241 False Positives (FP), True Negatives (TN) and False Negatives (FN). To complement  
 242 the non-spatial information provided by the ROC curves, we opted to project these four  
 243 values over the geographic space, producing in turn a confusion map (Titti et al., 2022).

244 We used these metrics in a number of performance tests. Specifically, we initially  
 245 tested our best model, built according to the description provided in Section 2.2, and  
 246 then considered it as our reference to compared against two additional cross-validation  
 247 schemes. One corresponds to a purely random 10-fold cross validation (RCV hereafter),  
 248 where 10% of the slope units are randomly extracted for testing, constraining the selec-  
 249 tion just once per mapping units, over ten subsequent replicates. The idea behind this  
 250 validation routine is for us to assess performance while the data is perturbed the least.  
 251 In fact, the random selection essentially keeps the residual spatial dependence, if any,  
 252 almost intact. For this reason, the performance is expected to remain close to the ref-  
 253 erence model. Instead, to really grasp how well a model is capable of performing a sus-  
 254 ceptibility prediction task, one should always include a spatially-constrained cross-validation  
 255 (SCV). A rich description on why and how to implement this technique can be found  
 256 in Brenning (2012) and Pohjankukka et al. (2017). Here we briefly mention that a spa-  
 257 tial cross-validation boils down to testing the model capabilities in an unknown region,  
 258 thus in a context where the model is blind to any potential landslide clustering effect or  
 259 residual spatial dependence. In turn, this usually leads to lower performance compared

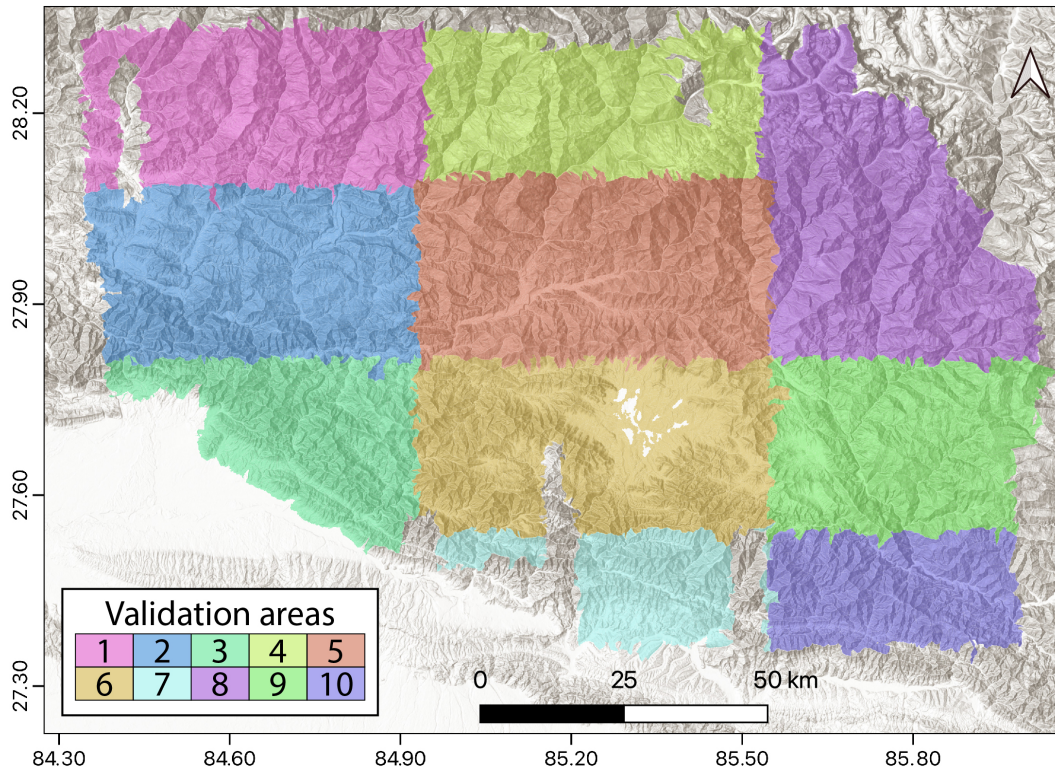


**Figure 3.** Aggregation of the slope unit partition into ten subregions, used for spatial cross-validation purposes.

260 to the reference model but also offers an overview of what to expect in one of the worst  
 261 cases a classifier can face. In this work we implemented our SCV by dividing the area  
 262 into ten sub-regions according to a squared lattice. Then, all the slope units falling within  
 263 one area were used for testing while the remaining nine were used for calibration. This  
 264 routine has been repeated ten times, until covering the whole study area and testing all  
 265 the slope units partitioning it (see Figure 3).

#### 266 **2.4 Interactive demonstration through a web application**

267 Explaining the potential of our ExAI simply through scientific illustrations may  
 268 have not offered the same understanding as an interactive tool. For this reason, we have  
 269 opted for a web application where our model results can be interactively queried to of-  
 270 fer a more immersive experience to the readers and to anybody interested in it. The web-  
 271 GIS is meant to provide the same level of query as it will be shown in the other figures  
 272 in this manuscript. In addition to that, the same operation could be repeated for any  
 273 slope unit in our study area, letting any user grasp why our ExAI assigned a given prob-  
 274 ability value as a linear combination of weights estimated for each predictor multiplied  
 275 by their predictor value at specific locations.

276 Our web-GIS relies on a ArcGIS online platform, using a standard ESRI template  
 277 for web applications. The ExAI output was computed outside the platform, a figure for  
 278 every SU created in python and then stored in a repository where our web-GIS goes to  
 279 pick any element queried by the user. When mentioning our choice of a relatively coarse  
 280 slope unit partition in the previous section, we should also stress that a finer partition  
 281 would have also required generating a much larger number of images, one for each slope



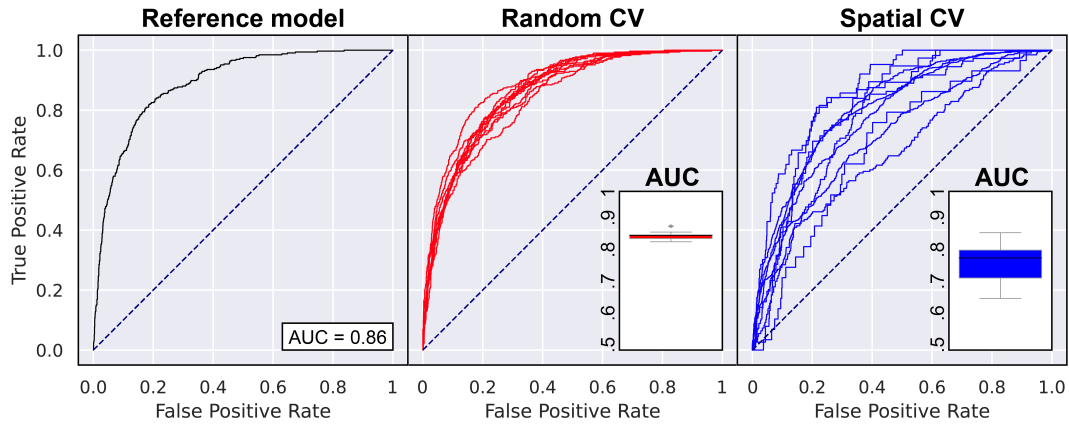


**Figure 4.** Panels from left to right: ROC curve and associated AUC of our reference ExAI model; ten ROC curves generated through a purely random cross-validation, with associated AUC values boxplotted at the bottom; ten ROC curves generated through spatial cross-validation, with associated AUC values boxplotted at the bottom.

282 unit, increasing the data storage requirements beyond the scope of a demonstrational  
 283 online platform.

### 284 3 Results

285 Below we will initially report our ExAI performance, after which we will provide  
 286 an extensive description of how the ExAI can be queried to understand why a specific  
 287 probability value has been assigned to a slope unit. Ultimately, we conclude this section  
 288 by illustrating our web application.

### 289 4 Performance overview

290 The most common characteristic of a machine/deep learning tools is their predic-  
 291 tion capacity. Figure 4, offers an overview of our modeling performance. Specifically, our  
 292 reference model falls in the excellent performance class according to Hosmer and Lemeshow  
 293 (2000). This is also the case for the RCV, with a mean AUC of 0.86 and a very limited  
 294 spread measured in a single standard deviation of 0.01. As mentioned in Section 2.3, the  
 295 SCV procedure is where one would expect a significant drop in performance. This is the  
 296 case also here, with a mean AUC of 0.77 and a standard deviation of 0.06. This still means  
 297 that on average our model still is very close to the excellent performance class accord-  
 298 ing to (Hosmer & Lemeshow, 2000). However, it points out at local performance defi-  
 299 ciencies with a minimum AUC of 0.66.

300 Interestingly, this low performance is achieved for the tenth sub-region shown in  
 301 Figure 3. The south-easter sector of the study area is also the one that was shaken the  
 302 least by the Gorkha earthquake and this is likely the reason why our coseismic ExAI sus-  
 303 ceptibility model struggled there.

304 Similar considerations emerge also when looking at the three confusion maps shown  
 305 in Figure 5. There, the spatial pattern of TP and FN essentially stay the same for the  
 306 reference model as well as the two cross-validation schemes. This is an indicator of the  
 307 consistent capacity of our ExAI to recognize unstable slope units. The main difference  
 308 among the three maps becomes evident when looking at how FP substitute the TN. This  
 309 is something that may be considered an issue at a first glance. However, we should re-

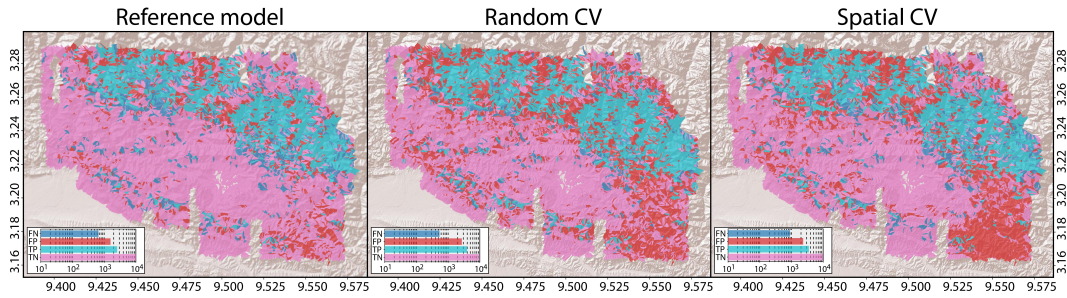


**Figure 5.** Confusion maps for the reference model and the two cross-validations we tested. The barplots correspond to the relative confusion matrices.

310 call that FP correspond to slope units that did not have a landslide in the original dataset  
 311 but that the model deemed to be unstable. In other words, this is not an issue that should  
 312 raise questions on the quality of our classifier. Conversely, it should be considered an in-  
 313 dication of locations that may have not generated landslides in the occasion of the Gorkha  
 314 earthquake but could still fail in the future.

## 315 5 Looking into the ExAI

316 Recent advancements in Artificial Intelligence have significantly pushed the bound-  
 317 aries of what can be queried and visualized out of an explainable AI. In this work, we  
 318 tried to provide several options for the readers and selected the one we considered to be  
 319 the best for our web application.

320 The simplest way of understanding why a given AI has assigned a specific label to  
 321 a mapping unit can be done by examining the variable importance (Gunning et al., 2019;  
 322 Aguilera et al., 2022). This measure expresses the influence of each predictor used in the  
 323 model with respect to the others and has already found a few applications in data-driven  
 324 natural hazard models (Stumpf & Kerle, 2011; J. Goetz et al., 2015; Steger et al., 2016).  
 325 Here we re-created a variable importance plot in Figure 6, by using the computed SHAP  
 326 values. The mean slope per slope unit and the peak ground velocity are shown to dom-  
 327 inate the probability estimation. Then, the remaining six predictors appear to exert a  
 328 similar influence onto the final susceptibility.

329 Another already available tool to visualize overall predictor's influence consists of  
 330 response plots (Merow et al., 2013). This tool has also been featured in a number of nat-  
 331 ural hazard (Vorpahl et al., 2012; Lombardo, Fubelli, et al., 2016; Lombardo, Bachofer,  
 332 et al., 2016) applications albeit to a lesser extent compared to the variable importance  
 333 presented above. In this work, we re-proposed a response plot graphical summary by plot-  
 334 ting SHAP values against each predictor's domain. This is shown in Figure 7 where the  
 335 two dominant predictors in the model appear to be again the mean slope steepness ( $Slp_m$ )  
 336 and the mean peak ground velocity ( $PGV_{Usgs}$ ) per slope unit.

337 The last two illustrations have been routinely included in a number of articles al-  
 338 ready for over a decade. However, this has not been sufficient to label any standard AI  
 339 as explainable. The reason is due to the static vision these tools provide with respect  
 340 to the modeling result. In fact, they essentially tell the same story, this being two pre-  
 341 dictors influencing more than others the final output. But, no other relevant informa-  
 342 tion can be retrieved on how this happens. In other words, these plot lack the capacity  
 343 to provide insight into how each predictor interacts with the others for each mapping units,  
 344 leading to the final probability value. This is where our ExAI enters an uncharted ter-  
 345 ritory in geosciences, providing a full description of these predictors' interactions. Be-

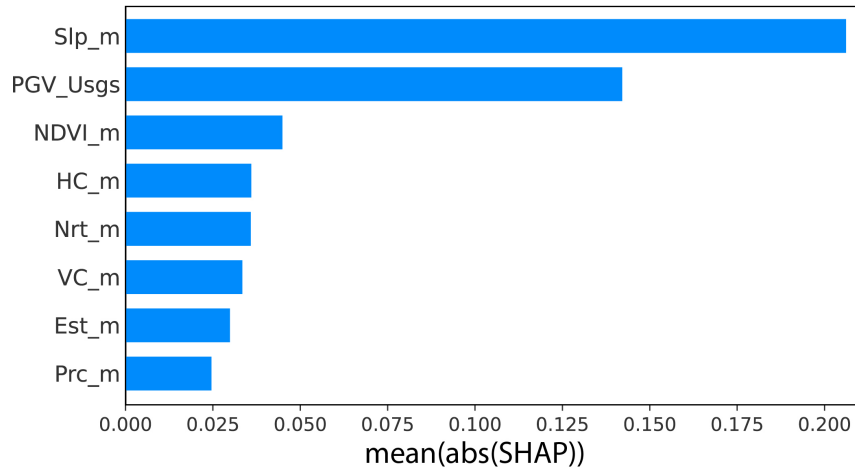


**Figure 6.** Variable importance plot obtained by taking the mean absolute value of SHAP, then ranked from the highest to the lowest contributor.

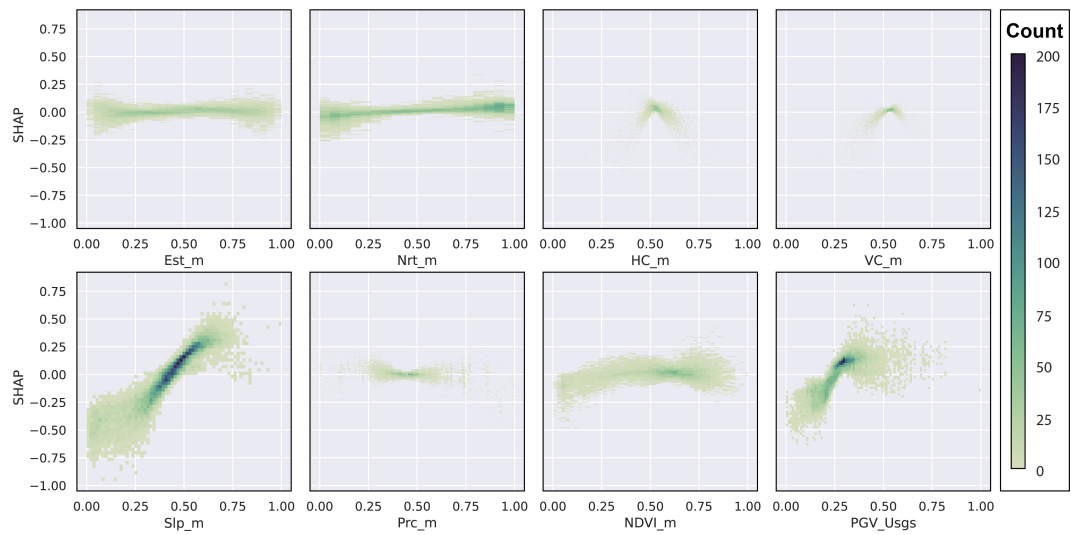


**Figure 7.** Response plots for each of the predictors used in the model. The x-axis reports the rescaled domain of each predictor while the y-axis corresponds to the influence each predictor exerted onto the susceptibility estimates.

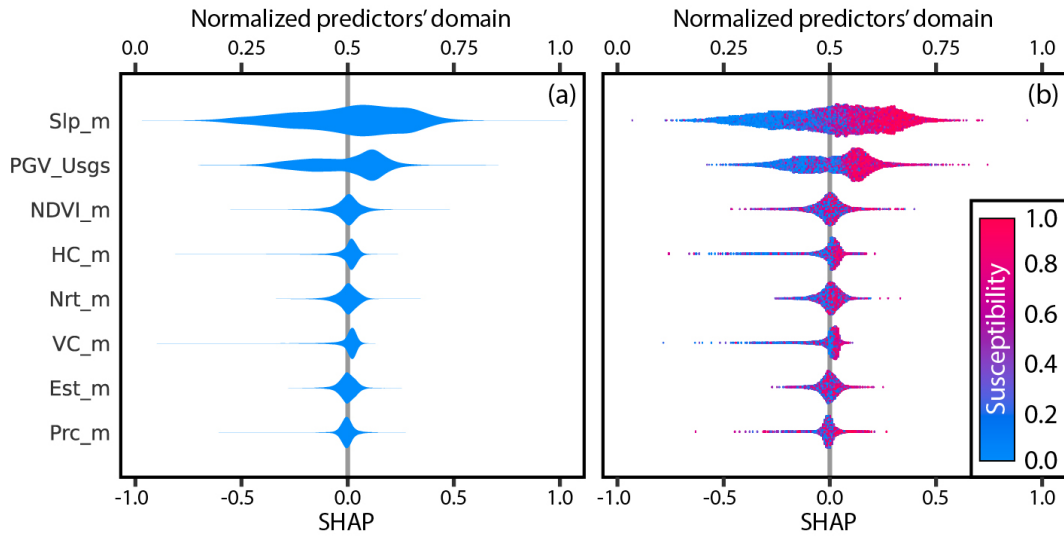


**Figure 8.** Panel (a) shows the SHAP distribution for each predictor expressed with a violin plot obtained considering all slope units. Panel (b) does the same but each dot corresponding to a specific slopes unit has been further colored with the susceptibility it was ultimately assigned with.

low we will provide tools to do so, presented in order of the level of information they provide.

The simplest way to additionally explore our ExAI is shown in Figure 8, at an information level which is not far off from the one provided by the two illustrations above. Specifically, panel (a) shows the overall SHAP distribution per predictor computed for the whole study area. This is something very similar to what was shown in Figure 7, to which we start adding information on specific locations. Panel (b) does exactly this task by showing the actually probability assigned to each slope unit (or dot in the figure). As a result, one can start seeing that SHAP values computed for single predictors assume essentially an alternating coloration per slope units until the mean NDVI ( $NVDI_m$ ), after which an increase  $PGV_{Usgs}$  and  $Slp_m$  and associated SHAP values, also corresponds in an increase in susceptibility. This indicates a dominant effect of the last two predictors, which is a similar conclusion to what showed in previous illustrations. However, it already provides an indication that our ExAI will delve much deeper than usual tools, away from a single perspective over the whole study area and much closer to what happens at the level of the single slope unit.

The level of the single mapping unit is actually where our ExAI aims to provide information to the end user. This can be shown in Figure 9, where two slope units have been extracted as an example for demonstration. Panel (a) shows how the final susceptibility of 0.23 was reached adding the contributions of all predictors to the base probability of 0.42. We briefly point out here that 0.42 is the starting value as a result of the balanced presence/absence data we opted for. Any further imbalance in the proportion of stable and unstable slope units would lead to a lower starting value (see Frattini et al., 2010; Lombardo & Mai, 2018). Going back to Figure 9, this graphical summary is the perfect example to deliver how powerful is an ExAI, to the point where one can assess whether the susceptibility makes sense for single mapping units. However, generating these plots for each mapping unit may be too complex. For this reason, it is possible to simplify the graph while reporting the same information.

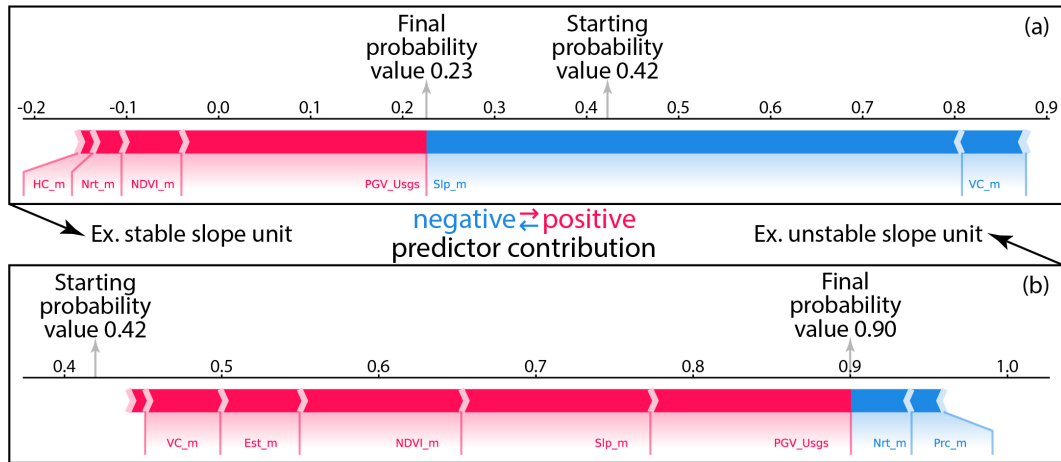


**Figure 9.** Panel (a) shows an example of a slope unit that started with a 0.42 probability value and whose final susceptibility reached 0.23. This value was reached due to the contribution of the other predictors, whose sign is graphically summarized through the horizontal arrows' direction and the magnitude is depicted through the horizontal arrows' length. The same is shown in panel (b) for a slope unit that started with a base probability of 0.42 and reached a final susceptibility estimate of 0.9.

374 This simpler yet effective overview is provided in Figure 10. There, in panel (a) we  
 375 propose once more the same information provided in Figure 9 for two slope units. The  
 376 way this plot can be read is to start from the bottom, where again the base susceptibil-  
 377 ity is 0.42 and then monitor the variations brought by each predictor listed on the y-axis.  
 378 As for panel (b), we plotted it to demonstrate that this type of plotting makes it pos-  
 379 sible to compare as many slope unit as one desires.

380 The ExAI proposed by Lundberg and Lee (2017) suggests even more tools to vi-  
 381 sualize the model output. However, we consider the last illustration to be the most ef-  
 382 fective among all the available ones. For this reason, we have equipped our web appli-  
 383 cation precisely with this type of visualization. The app can be accessed at the follow-  
 384 ing link: <https://arcg.is/0unziD>. There, we have placed the final susceptibility map pro-  
 385 duced by our ExAI (see Figure 11).

386 Each mapping unit that constitutes the map can then be interactively queried. Specif-  
 387 ically, by clicking on any slope unit, the system plots the ExAI according to the style  
 388 explained above.

389 Below we present to examples captured from two adjacent SUs. Figures 12 and 13  
 390 provide two examples of how to visualize the ExAI decision within our web application,  
 391 for two SUs estimated to be unstable and stable, respectively.

## 392 6 Discussion

393 The model we present relied on a relative small number of predictors. We opted  
 394 for this structure to offer a simple and efficient visualization of the ExAI decisions. This  
 395 characteristics has led our ExAI to highlight minimal contributions of terrain charac-  
 396 teristics other that the slope steepness, in addition to which the ground motion deter-  
 397 mines most of the final probability. Nevertheless, this already provides a good idea of what ExAI  
 398 can do and how its decisions can be queried in depth to understand the extent to which

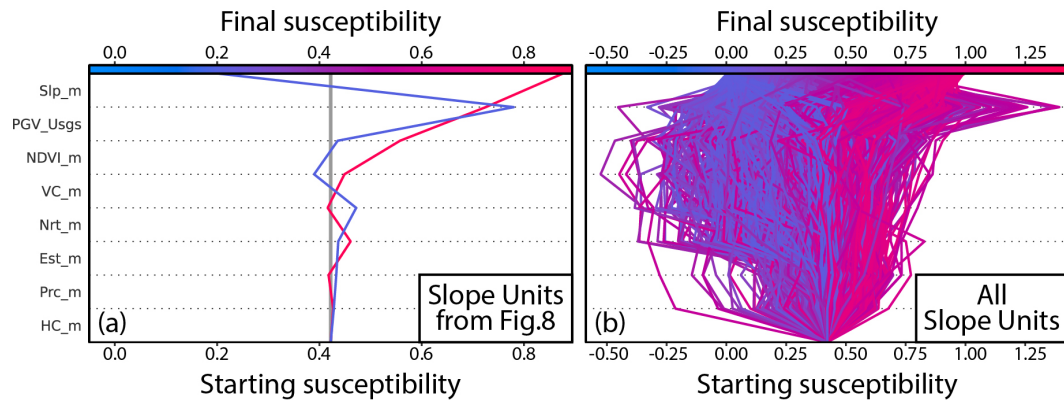


**Figure 10.** Panel (a) summarizes all the information presented in Figure 9 in a much more straightforward way. The variation of the probability estimates for the two slope units is compressed in a single line plot. Panel (b) makes it possible to present the whole information for all slope units partitioning the study area.

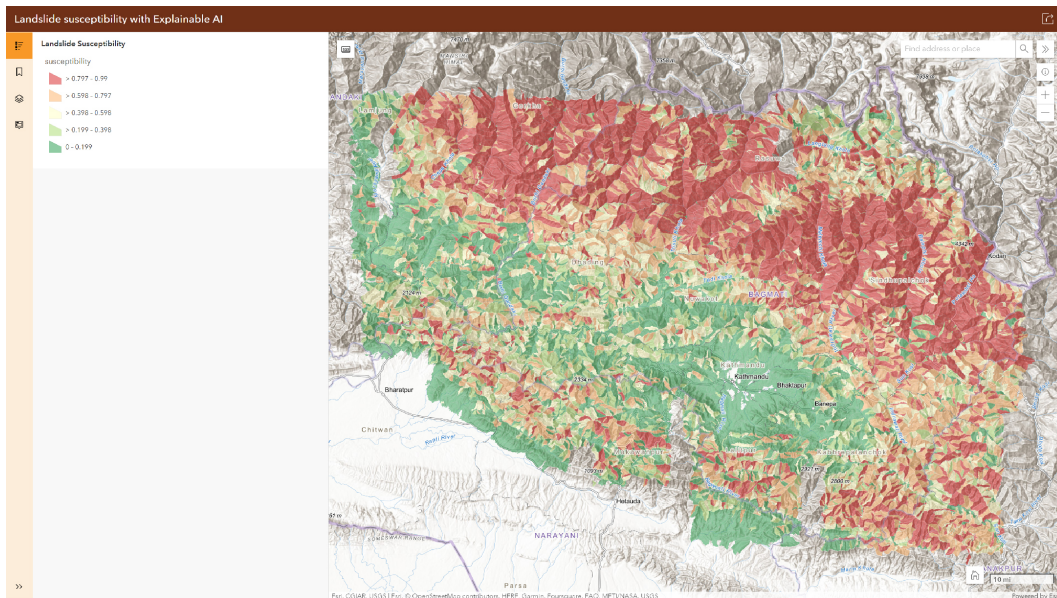


**Figure 11.** General overview of the web application. The susceptibility map we obtained by using our ExAI is depicted here into five equal spaced classes.

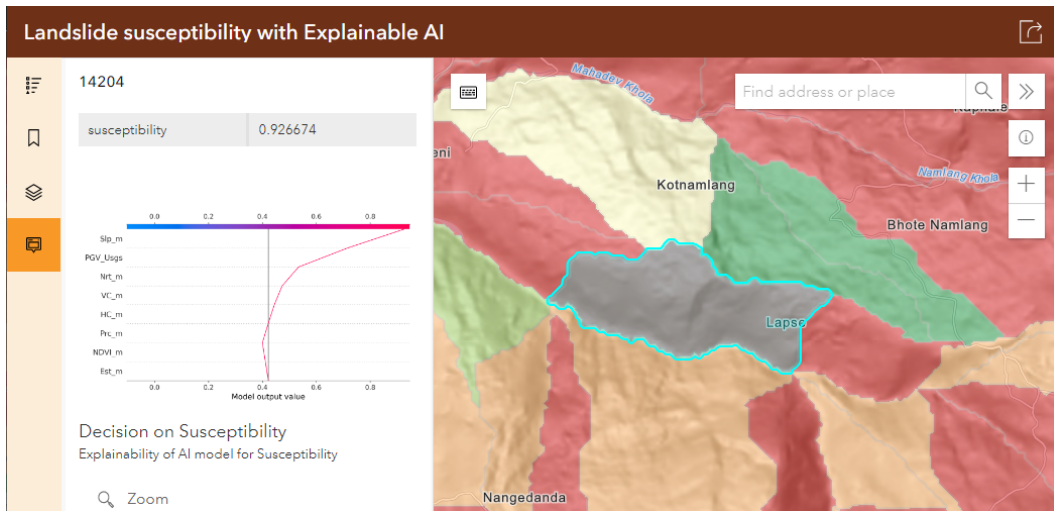


**Figure 12.** Example of an ExAI query for an unstable SU.

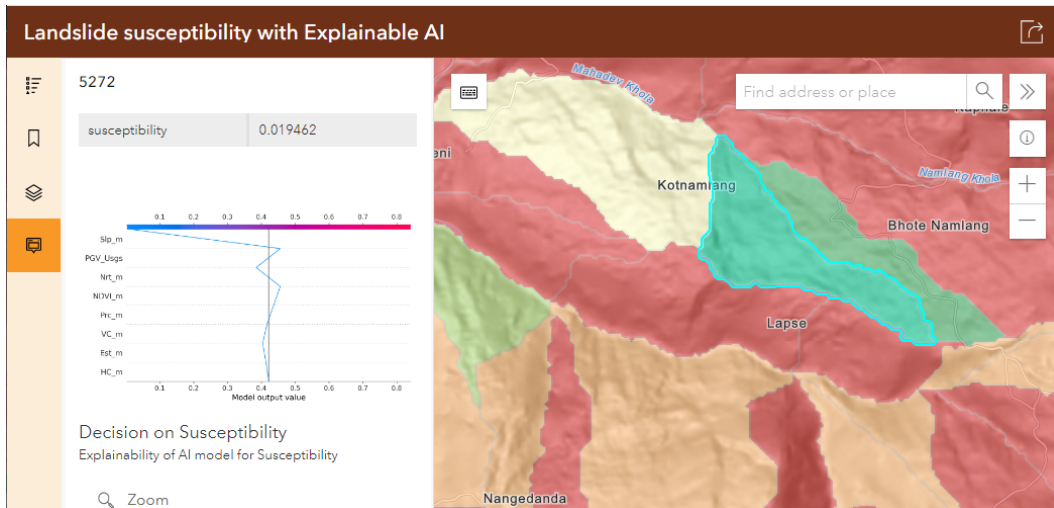


**Figure 13.** Example of an ExAI query for a stable SU.

399 one can trust the maps it produces. The traditional variable importance plot in fact, is  
 400 unsuitable to provide the whole picture. Figure 6 simply illustrates the extent to which  
 401 each variable dominates the outcome. However, it does not tell the user whether this makes  
 402 sense from an interpretative standpoint. For instance, it indeed makes sense that  $Slp_m$   
 403 and  $PGV_{Usgs}$  does control most of the probability of landslide occurrence for the co-seismic  
 404 example we considered in this work. However, the artificial intelligence behind could in-  
 405 crease the probability at decreasing values of slope steepness and/or ground motion; some-  
 406 thing that would violate our basic understanding of the physics behind the genesis of a  
 407 the failure mechanism. For this reason, response plots like Figure 7 add another level  
 408 of understanding for they allow to monitor variations in SHAP with respect to each pre-  
 409 dictors' domain. This is a capability which is typical of statistical models (Lima et al.,  
 410 2021; Tanyaş et al., 2022) and has found very few applications in machine learning (Park,  
 411 2015; Vorpahl et al., 2012). However, even in this case, the level of information provided  
 412 is very generic and corresponds to the overall behaviour of each predictor with respect  
 413 to the entire map it contributes to define. An analogous graphical representation of the  
 414 model output is shown in Figure 8(a). And even if panel (b) adds some additional in-  
 415 formation through the embedded colorcoding, the model could still be locally mistak-  
 416 ing the effect of certain predictors. In fact, at the local level, no traditional statistical  
 417 models nor machine/deep learning ones have so far provided a transparent understand-  
 418 ing of predictors contributions and how they specifically interact with each other. This  
 419 aspect is now achievable through ExAI and Figures such as 9 and 10 provides a clear rep-  
 420 resentation of how this can be translated into meaningful scientific illustrations. These  
 421 types of graphical summaries have they have been created with the idea in mind of mak-  
 422 ing black boxes into white ones. At this local level, here expressed through SUs, one can  
 423 examine how reliable the probabilistic estimates are. For instance, to continue the  $Slp_m$   
 424 and  $PGV_{Usgs}$  example mentioned above, one can query a given SU, check the SHAP value  
 425 and then easily cross-reference it with respect to the actual steepness and ground mo-  
 426 tion values. As a result, one can interactively realize whether steeper slopes have been  
 427 assigned with a higher susceptibility or not. And, whether slopes that have undergone  
 428 a greater shaking have also been estimated with a higher likelihood to host a landslide.  
 429 The same is valid in the opposite situation and in any other level in between. In short,  
 430 ExAI provides a window into the core calculations that the given model has gone through,  
 431 helping the user to understand the extent to which the AI can be relied on. All this is  
 432 essentially possible in near-real-time and our web-application is meant to highlight this  
 433 specific characteristic. There, any user can query our model in a transparent manner that  
 434 has not yet been reached so far within the geoscientific community. And, which we hope  
 435 can become a standard as the use of ExAI becomes more common in the future.

436 We conclude by stressing that artificially intelligent models are usually acclaimed  
 437 due to their predictive capacity, which here we tested via a suite of validation routines.  
 438 The results shown in Figure 4 highlight predictive performance in line with other ma-  
 439 chine/deep learning studies, especially considering the limited number of predictors we  
 440 opted for in this work. An important element the same figure highlights is the fact that  
 441 despite Brenning (2012) clearly advocated for spatial cross-validations to become a stan-  
 442 dard in susceptibility modeling, this is something which is rarely done. And yet, a spa-  
 443 tial cross-validation constitutes an important element to really assess the extent to which  
 444 a given data-driven model can be used to predict natural hazard occurrences in areas  
 445 outside the training set. This is an important characteristic that goes beyond the explain-  
 446 ability or not of a given model, but it allows to estimate the minimum (worst-case sce-  
 447 nario) one could expect when transferring the prediction elsewhere.

## 448 7 Conclusions

449 Explainable artificially intelligence represents the future of data-driven models in  
 450 any scientific area. The prediction capacity of complex modeling architectures can be



451 dissected into its simpler elements, allowing one to understand the reason behind a model  
 452 result, leaving behind the negative connotation of the black box label and finally open-  
 453 ing up towards white box characteristics even in the context of machine/deep learning.

454 Our work here introduces ExAI for landslide prediction and it is meant to offer an  
 455 overview of the potential that this new generation of models can offer and will certainly  
 456 offer in the future. We see ExAI as a milestone in the history of data-driven models and  
 457 the extent to which these models may change the way we perceive artificially intelligent  
 458 decisions is yet to be unraveled. However, we also see an opening for improvements. Cur-  
 459 rently, and this is also valid in this manuscript, ExAI is mainly integrated as part of bi-  
 460 nary classifiers. However, the information of where landslides may occur is not the only  
 461 important element in the chain of hazard assessment. Another important notion would  
 462 be estimating how large landslides may be once they trigger on a slope labeled as un-  
 463 stable. Few data-driven models have already been proposed to address this issue and we  
 464 see the next step to do the same in the context of ExAI, where the expected dimension  
 465 of a landslide can be precisely predicted while contextually providing information on why  
 466 it may reach that extent.

467 Similar considerations can be extended to estimate potential losses and open up  
 468 this framework towards societal risk modeling. And again, similar considerations can be  
 469 extended to beyond the pure spatial context and towards spatio-temporal modeling.

470 In summary, ExAI applications are at an infancy stage and much is to be explored  
 471 on what can be improved and how their use can be directed to address other research  
 472 questions. In this work, we hoped to highlight its strength and stimulate the spread of  
 473 ExAI even further. For this specific reason, we have build an interactive demonstration  
 474 accessible at <https://arcg.is/0unziD>. Moreover, to promote reproducibility and repeata-  
 475 bility, data and codes have also been shared in a FAIR complying repository ([https://](https://doi.org/10.5281/zenodo.6976122)  
 476 [doi.org/10.5281/zenodo.6976122](https://doi.org/10.5281/zenodo.6976122)) (Dahal & Lombardo, 2022).

## 477 Acknowledgments

478 Ashok Dahal has implemented the ExAI, run all the analyses and created the web-GIS  
 479 platform. Luigi Lombardo has worked on drafting the manuscript. Landslides are avail-  
 480 able at: <https://www.sciencebase.gov/catalog/item/583f4114e4b04fc80e3c4a1a>, whereas  
 481 data and codes to reproduce our ExAI can be found at: [https://doi.org/10.5281/](https://doi.org/10.5281/zenodo.6976122)  
 482 [zenodo.6976122](https://doi.org/10.5281/zenodo.6976122) (Dahal & Lombardo, 2022).

## 483 References

- 484 Aguilera, Q., Lombardo, L., Tanyas, H., & Lipani, A. (2022). On the prediction  
 485 of landslide occurrences and sizes via Hierarchical Neural Networks. *Stochastic*  
 486 *Environmental Research and Risk Assessment*, 1–18.
- 487 Alvioli, M., Guzzetti, F., & Marchesini, I. (2020, June). Parameter-free delineation  
 488 of slope units and terrain subdivision of Italy. *Geomorphology*, 358, 107124.  
 489 Retrieved 2021-08-30, from [https://www.sciencedirect.com/science/](https://www.sciencedirect.com/science/article/pii/S0169555X20300969)  
 490 [article/pii/S0169555X20300969](https://www.sciencedirect.com/science/article/pii/S0169555X20300969) doi: 10.1016/j.geomorph.2020.107124
- 491 Alvioli, M., Marchesini, I., Reichenbach, P., Rossi, M., Ardizzone, F., Fiorucci, F.,  
 492 & Guzzetti, F. (2016). Automatic delineation of geomorphological slope  
 493 units with r.slopeunits v1.0 and their optimization for landslide susceptibility  
 494 modeling. *Geoscientific Model Development*, 9(11), 3975–3991.
- 495 Amato, G., Eisank, C., Castro-Camilo, D., & Lombardo, L. (2019). Accounting for  
 496 covariate distributions in slope–unit–based landslide susceptibility models. a  
 497 case study in the alpine environment. *Engineering geology*, 260, 105237.
- 498 Atkinson, P., Jiskoot, H., Massari, R., & Murray, T. (1998). Generalized linear mod-  
 499 elling in geomorphology. *Earth Surface Processes and Landforms: The Journal*

- 500       of the *British Geomorphological Group*, 23(13), 1185–1195.
- 501     Atkinson, P. M., & Massari, R. (1998). Generalised linear modelling of suscepti-  
502       bility to landsliding in the central Apennines, Italy. *Computers & Geosciences*,  
503       24(4), 373–385.
- 504     Baldi, P., & Sadowski, P. J. (2013). Understanding dropout. *Advances in neural in-*  
505       *formation processing systems*, 26.
- 506     Ballabio, C., & Sterlacchini, S. (2012). Support vector machines for landslide suscep-  
507       tibility mapping: the Staffora River Basin case study, Italy. *Mathematical geo-*  
508       *sciences*, 44(1), 47–70.
- 509     Bednarik, M., & Pauditš, P. (2010). Different ways of landslide geometry interpre-  
510       tation in a process of statistical landslide susceptibility and hazard assessment:  
511       Horná súča (western slovakia) case study. *Environmental Earth Sciences*,  
512       61(4), 733–739.
- 513     Brabb, E., Pampeyan, H., & Bonilla, M. (1972). MG 1972. landslide susceptibility in  
514       San Mateo County, California. *US Geological Survey Miscellaneous Field Stud-*  
515       *ies Map MF-360, scale, 1(62,500)*.
- 516     Brenning, A. (2008). Statistical geocomputing combining r and SAGA: The example  
517       of landslide susceptibility analysis with generalized additive models. *Ham-*  
518       *burger Beiträge zur Physischen Geographie und Landschaftsökologie*, 19(23-32),  
519       410.
- 520     Brenning, A. (2012). Spatial cross-validation and bootstrap for the assessment of  
521       prediction rules in remote sensing: The R package sperrorest. In *2012 ieee in-*  
522       *ternational geoscience and remote sensing symposium* (pp. 5372–5375).
- 523     Bui, D. T., Tsangaratos, P., Nguyen, V.-T., Van Liem, N., & Trinh, P. T. (2020).  
524       Comparing the prediction performance of a Deep Learning Neural Network  
525       model with conventional machine learning models in landslide susceptibility  
526       assessment. *Catena*, 188, 104426.
- 527     Carrara, A. (1983). Multivariate models for landslide hazard evaluation. *Journal of*  
528       *the International Association for Mathematical Geology*, 15(3), 403–426.
- 529     Carrara, A., Cardinali, M., Guzzetti, F., & Reichenbach, P. (1995). GIS technology  
530       in mapping landslide hazard. In *Geographical information systems in assessing*  
531       *natural hazards* (pp. 135–175). Springer.
- 532     Castro Camilo, D., Lombardo, L., Mai, P., Dou, J., & Huser, R. (2017). Han-  
533       dling high predictor dimensionality in slope–unit–based landslide susceptibility  
534       models through LASSO–penalized Generalized Linear Model. *Environmental*  
535       *Modelling and Software*, 97, 145–156.
- 536     Catani, F., Lagomarsino, D., Segoni, S., & Tofani, V. (2013). Landslide susceptibil-  
537       ity estimation by random forests technique: sensitivity and scaling issues. *Nat-*  
538       *ural Hazards and Earth System Sciences*, 13(11), 2815–2831.
- 539     Dahal, A., & Lombardo, L. (2022, August). *Data: Explainable artificial intelligence*  
540       *in geoscience: a glimpse into the future of landslide susceptibility modeling*.  
541       Zenodo. Retrieved from <https://doi.org/10.5281/zenodo.6976122> doi:  
542       10.5281/zenodo.6976122
- 543     Das, I., Stein, A., Kerle, N., & Dadhwal, V. K. (2012). Landslide susceptibility  
544       mapping along road corridors in the Indian Himalayas using Bayesian logis-  
545       tic regression models. *Geomorphology*, 179, 116–125. doi: [https://doi.org/](https://doi.org/10.1016/j.geomorph.2012.08.004)  
546       10.1016/j.geomorph.2012.08.004
- 547     Dhakal, A. S., Amada, T., Aniya, M., et al. (2000). Landslide hazard mapping and  
548       its evaluation using GIS: an investigation of sampling schemes for a grid-cell  
549       based quantitative method. *Photogrammetric engineering and remote sensing*,  
550       66(8), 981–989.
- 551     Fang, Z., Wang, Y., Peng, L., & Hong, H. (2020). Integration of convolutional neural  
552       network and conventional machine learning classifiers for landslide susceptibil-  
553       ity mapping. *Computers & Geosciences*, 139, 104470.
- 554     Frattini, P., Crosta, G., & Carrara, A. (2010). Techniques for evaluating the perfor-

- mance of landslide susceptibility models. *Engineering Geology*, *111*(1), 62–72. doi: <https://doi.org/10.1016/j.enggeo.2009.12.004>
- Funk, C., Peterson, P., Landsfeld, M., Pedreros, D., Verdin, J., Shukla, S., . . . others (2015). The climate hazards infrared precipitation with stations—a new environmental record for monitoring extremes. *Scientific data*, *2*(1), 1–21.
- Gates, W. E., & Heil, R. J. (1980). Geographic information systems. *Journal of the Surveying and Mapping Division*, *106*(1), 105–117.
- Goetz, J., Brenning, A., Petschko, H., & Leopold, P. (2015). Evaluating machine learning and statistical prediction techniques for landslide susceptibility modeling. *Computers & geosciences*, *81*, 1–11.
- Goetz, J. N., Guthrie, R. H., & Brenning, A. (2011). Integrating physical and empirical landslide susceptibility models using generalized additive models. *Geomorphology*, *129*(3–4), 376–386.
- Gunning, D., Stefik, M., Choi, J., Miller, T., Stumpf, S., & Yang, G.-Z. (2019). XAI—Explainable artificial intelligence. *Science robotics*, *4*(37), eaay7120.
- Guzzetti, F., Reichenbach, P., Ardizzone, F., Cardinali, M., & Galli, M. (2006). Estimating the quality of landslide susceptibility models. *Geomorphology*, *81*(1–2), 166–184. doi: [10.1016/j.geomorph.2006.04.007](https://doi.org/10.1016/j.geomorph.2006.04.007)
- Heerdegen, R. G., & Beran, M. A. (1982). Quantifying source areas through land surface curvature and shape. *Journal of Hydrology*, *57*(3–4), 359–373.
- Hosmer, D. W., & Lemeshow, S. (2000). *Applied Logistic Regression* (2nd ed ed.). New York: Wiley.
- Hua, Y., Wang, X., Li, Y., Xu, P., & Xia, W. (2021). Dynamic development of landslide susceptibility based on slope unit and deep neural networks. *Landslides*, *18*(1), 281–302.
- Ioffe, S., & Szegedy, C. (2015). Batch normalization: Accelerating deep network training by reducing internal covariate shift. In *International conference on machine learning* (pp. 448–456).
- Kingma, D. P., & Ba, J. (2014). Adam: A method for stochastic optimization. *arXiv preprint arXiv:1412.6980*.
- Li, X., & Claramunt, C. (2006). A spatial entropy-based decision tree for classification of geographical information. *Transactions in GIS*, *10*(3), 451–467.
- Lima, P., Steger, S., & Glade, T. (2021). Counteracting flawed landslide data in statistically based landslide susceptibility modelling for very large areas: a national-scale assessment for Austria. *Landslides*, 1–16.
- Lombardo, L., Bachofer, F., Cama, M., Märker, M., & Rotigliano, E. (2016). Exploiting Maximum Entropy method and ASTER data for assessing debris flow and debris slide susceptibility for the Giampilieri catchment (north-eastern Sicily, Italy). *Earth Surface Processes and Landforms*, *41*(12), 1776–1789.
- Lombardo, L., Fubelli, G., Amato, G., & Bonasera, M. (2016). Presence-only approach to assess landslide triggering–thickness susceptibility: a test for the Mili catchment (north-eastern Sicily, Italy). *Natural Hazards*, *84*(1), 565–588.
- Lombardo, L., & Mai, P. M. (2018). Presenting logistic regression-based landslide susceptibility results. *Engineering geology*, *244*, 14–24.
- Lombardo, L., Saia, S., Schillaci, C., Mai, P. M., & Huser, R. (2018). Modeling soil organic carbon with Quantile Regression: Dissecting predictors’ effects on carbon stocks. *Geoderma*, *318*, 148–159. doi: <https://doi.org/10.1016/j.geoderma.2017.12.011>
- Lombardo, L., & Tanyas, H. (2020). Chrono-validation of near-real-time landslide susceptibility models via plug-in statistical simulations. *Engineering Geology*, *278*, 105818.
- Lombardo, L., & Tanyas, H. (2021). From scenario-based seismic hazard to scenario-based landslide hazard: fast-forwarding to the future via statistical simulations. *Stochastic Environmental Research and Risk Assessment*, 1–14.

- 610 Lundberg, S. M., & Lee, S.-I. (2017). A Unified Approach to Interpreting Model  
 611 Predictions. In I. Guyon et al. (Eds.), *Advances in neural information pro-*  
 612 *cessing systems 30* (pp. 4765–4774). Curran Associates, Inc. Retrieved  
 613 from [http://papers.nips.cc/paper/7062-a-unified-approach-to-](http://papers.nips.cc/paper/7062-a-unified-approach-to-interpreting-model-predictions.pdf)  
 614 [-interpreting-model-predictions.pdf](http://papers.nips.cc/paper/7062-a-unified-approach-to-interpreting-model-predictions.pdf)
- 615 Marmion, M., Hjort, J., Thuiller, W., & Luoto, M. (2009). Statistical consensus  
 616 methods for improving predictive geomorphology maps. *Computers & Geo-*  
 617 *sciences, 35*(3), 615–625.
- 618 Meena, S. R., Puliero, S., Bhuyan, K., Floris, M., & Catani, F. (2022). Assessing the  
 619 importance of conditioning factor selection in landslide susceptibility for the  
 620 province of Belluno (region of Veneto, northeastern Italy). *Natural hazards and*  
 621 *earth system sciences, 22*(4), 1395–1417.
- 622 Melchiorre, C., Matteucci, M., Azzoni, A., & Zanchi, A. (2008). Artificial neural net-  
 623 works and cluster analysis in landslide susceptibility zonation. *Geomorphology,*  
 624 *94*(3-4), 379–400.
- 625 Merow, C., Smith, M. J., & Silander Jr, J. A. (2013). A practical guide to MaxEnt  
 626 for modeling species' distributions: what it does, and why inputs and settings  
 627 matter. *Ecography, 36*(10), 1058–1069.
- 628 Naranjo, J. L., Van Westen, C., & Soeters, R. (1994). Evaluating the use of training  
 629 areas in bivariate statistical landslide hazard analysis-a case study in Colom-  
 630 bia. *ITC journal*(3), 292–300.
- 631 Nowicki Jesse, M., Hamburger, M., Allstadt, K., Wald, D., Robeson, S., Tanyas, H.,  
 632 ... Thompson, E. (2018). A Global Empirical Model for Near-Real-Time As-  
 633 sessment of Seismically Induced Landslides. *Journal of Geophysical Research:*  
 634 *Earth Surface, 123*(8), 1835–1859.
- 635 Park, N.-W. (2015). Using maximum entropy modeling for landslide susceptibility  
 636 mapping with multiple geoenvironmental data sets. *Environmental Earth Sci-*  
 637 *ences, 73*(3), 937–949.
- 638 Pettorelli, N., Vik, J. O., Mysterud, A., Gaillard, J.-M., Tucker, C. J., & Stenseth,  
 639 N. C. (2005). Using the satellite-derived NDVI to assess ecological responses  
 640 to environmental change. *Trends in ecology & evolution, 20*(9), 503–510.
- 641 Pohjankukka, J., Pahikkala, T., Nevalainen, P., & Heikkonen, J. (2017). Esti-  
 642 mating the prediction performance of spatial models via spatial k-fold cross  
 643 validation. *International Journal of Geographical Information Science, 31*(10),  
 644 2001–2019.
- 645 Pourghasemi, H. R., & Rossi, M. (2017). Landslide susceptibility modeling in a  
 646 landslide prone area in Mazandarn province, north of Iran: a comparison be-  
 647 tween GLM, GAM, MARS, and M-AHP methods. *Theoretical and Applied*  
 648 *Climatology, 130*(1), 609–633.
- 649 Rahmati, O., Kornejady, A., Samadi, M., Deo, R. C., Conoscenti, C., Lombardo, L.,  
 650 ... others (2019). Pmt: New analytical framework for automated evaluation  
 651 of geo-environmental modelling approaches. *Science of the total environment,*  
 652 *664*, 296–311.
- 653 Reichenbach, P., Rossi, M., Malamud, B., Mihir, M., & Guzzetti, F. (2018). A re-  
 654 view of statistically-based landslide susceptibility models. *Earth-Science Re-*  
 655 *views, 180*, 60–91. doi: 10.1016/j.earscirev.2018.03.001
- 656 Ribeiro, M. T., Singh, S., & Guestrin, C. (2016). " why should i trust you?" ex-  
 657 plaining the predictions of any classifier. In *Proceedings of the 22nd acm sigkdd*  
 658 *international conference on knowledge discovery and data mining* (pp. 1135–  
 659 1144).
- 660 Roback, K., Clark, M., West, A., Zekkos, D., Li, G., Gallen, S., ... Godt, J. (2017).  
 661 Map data of landslides triggered by the 25 April 2015 Mw 7.8 Gorkha,  
 662 Nepal earthquake. *US Geological Survey data release [data set], https://doi.*  
 663 *org/10.5066/F7DZ06F9.*
- 664 Roback, K., Clark, M. K., West, A. J., Zekkos, D., Li, G., Gallen, S. F., ... Godt,

- 665 J. W. (2018). The size, distribution, and mobility of landslides caused by the  
666 2015 Mw7.8 Gorkha earthquake, Nepal. *Geomorphology*, *301*, 121–138.
- 667 Schmidhuber, J. (2015). Deep learning in neural networks: An overview. *Neural net-*  
668 *works*, *61*, 85–117.
- 669 Soeters, R., & Van Westen, C. (1994). Slope instability: the role of remote sens-  
670 ing and GIS in recognition, analysis and zonation. In *Natural hazards and re-*  
671 *remote sensing* (pp. 44–50). Royal Society and Royal Academy of Engineering  
672 London.
- 673 Steger, S., Brenning, A., Bell, R., & Glade, T. (2016). The propagation of  
674 inventory–based positional errors into statistical landslide susceptibility mod-  
675 els. *Natural Hazards and Earth System Sciences*, *16*(12), 2729–2745. doi:  
676 10.5194/nhess-16-2729-2016
- 677 Štrumbelj, E., & Kononenko, I. (2014). Explaining prediction models and indi-  
678 vidual predictions with feature contributions. *Knowledge and information sys-*  
679 *tems*, *41*(3), 647–665.
- 680 Stumpf, A., & Kerle, N. (2011). Object-oriented mapping of landslides using Ran-  
681 dom Forests. *Remote sensing of environment*, *115*(10), 2564–2577.
- 682 Survey, U. G. (Ed.). (2015). *Landsat surface reflectance data* (Version 1: Orig-  
683 inally posted April 20, 2015; Version 1.1: June 16, 2015; Version 1.1 up-  
684 dated: March 27, 2019 ed.; Tech. Rep.). Reston, VA. Retrieved from  
685 <http://pubs.er.usgs.gov/publication/fs20153034> (Report) doi:  
686 10.3133/fs20153034
- 687 Tanyaş, H., van Westen, C., Allstadt, K., Nowicki, A. J. M., Görüm, T., Jibson, R.,  
688 ... Hovius, N. (2017). Presentation and Analysis of a Worldwide Database of  
689 Earthquake–Induced Landslide Inventories. *Journal of Geophysical Research:*  
690 *Earth Surface*, *122*(10), 1991–2015. doi: 10.1002/2017JF004236
- 691 Tanyaş, H., Hill, K., Mahoney, L., Fadel, I., & Lombardo, L. (2022). The world’s  
692 second-largest, recorded landslide event: Lessons learnt from the landslides  
693 triggered during and after the 2018 Mw 7.5 Papua New Guinea earthquake.  
694 *Engineering geology*, *297*, 106504.
- 695 Tanyaş, H., & Lombardo, L. (2020). Completeness Index for Earthquake–Induced  
696 Landslide Inventories. *Engineering geology*, *264*, 105331.
- 697 Titti, G., Sarretta, A., Lombardo, L., Crema, S., Pasuto, A., & Borgatti, L. (2022).  
698 Mapping susceptibility with open-source tools: a new plugin for QGIS. *Front*  
699 *Earth Sci*, *229*.
- 700 Titti, G., van Westen, C., Borgatti, L., Pasuto, A., & Lombardo, L. (2021). When  
701 Enough Is Really Enough? On the Minimum Number of Landslides to Build  
702 Reliable Susceptibility Models. *Geosciences*, *11*(11), 469.
- 703 Van Dao, D., Jaafari, A., Bayat, M., Mafi-Gholami, D., Qi, C., Moayedi, H., ... oth-  
704 ers (2020). A spatially explicit deep learning neural network model for the  
705 prediction of landslide susceptibility. *Catena*, *188*, 104451.
- 706 Van Zyl, J. J. (2001). The Shuttle Radar Topography Mission (SRTM): a break-  
707 through in remote sensing of topography. *Acta Astronautica*, *48*(5-12), 559–  
708 565.
- 709 Vorpahl, P., Elsenbeer, H., Märker, M., & Schröder, B. (2012). How can statistical  
710 models help to determine driving factors of landslides? *Ecological Modelling*,  
711 *239*, 27–39.
- 712 Worden, C., & Wald, D. J. (2016). ShakeMap manual online: Technical manual,  
713 user’s guide, and software guide. *US Geol. Surv.*, 1–156.
- 714 Yarotsky, D. (2017). Error bounds for approximations with deep ReLU networks.  
715 *Neural Networks*, *94*, 103–114.
- 716 Yesilnacar, E., & Topal, T. (2005). Landslide susceptibility mapping: a comparison  
717 of logistic regression and neural networks methods in a medium scale study,  
718 Hendek region (Turkey). *Engineering Geology*, *79*(3–4), 251–266.
- 719 Yi, Y., Zhang, Z., Zhang, W., Jia, H., & Zhang, J. (2020). Landslide susceptibility

720 mapping using multiscale sampling strategy and convolutional neural network:  
721 A case study in Jiuzhaigou region. *Catena*, 195, 104851.  
722 Zevenbergen, L. W., & Thorne, C. R. (1987). Quantitative analysis of land surface  
723 topography. *Earth surface processes and landforms*, 12(1), 47–56.